J. Fluid Mech. (1997), *vol.* 336, *pp.* 245–266

Excitation of secondary instabilities in boundary layers

By J. D. CROUCH

Boeing Commercial Airplane Group, PO Box 3707, Seattle, WA 98124-2207, USA

(Received 16 November 1995 and in revised form 6 November 1996)

The receptivity to fundamental and subharmonic secondary instabilities is analysed for two-dimensional boundary layers. Fundamental modes are excited by the direct scattering of Tollmien–Schlichting (TS) waves over surface variations. The excitation of subharmonic modes stems from the combined scattering of acoustic free-stream disturbances and TS waves over surface variations. The surface variations are localized in their streamwise extent and are the result of roughness or suction. The velocity field is expanded in terms of small parameters characterizing the acoustic disturbance and the surface variation. The TS wave is included as part of the base flow leading to a non-homogeneous system with periodic coefficients governing the receptivity. The receptivity amplitudes show a strong dependence on the TS-wave amplitude, and for subharmonic modes a strong dependence on the TS-wave phase at the location of the surface variation. The receptivity analysis shows a significant bias toward fundamental modes of secondary instability for larger TS-wave amplitudes – except for conditions of extremely high free-stream sound level. A combination of receptivity results and stability results suggests a bias toward subharmonic modes for TS-wave amplitudes below 0.5% and toward fundamental modes for TS-wave amplitudes above 0.5% (normalized by the local edge velocity).

1. Introduction

The onset of transition in boundary layers is often characterized by the development of a primary instability followed by the parametric excitation of secondary instabilities. For two-dimensional boundary layers at low Mach numbers, the dominant primary instability is a two-dimensional Tollmien–Schlichting (TS) wave. The initial bias toward two-dimensional waves results from a combination of larger growth rates and larger initial amplitudes. Once the two-dimensional wave reaches a significant amplitude it excites three-dimensional disturbances, which may otherwise be damped. These three-dimensional secondary instabilities have growth rates much larger than the initial primary modes, and, in some cases, lead rapidly to transition.

The ultimate occurrence and nature of transition, however, depend on the initial amplitudes of the disturbances. In the experiments of Saric & Thomas (1984), for example, different three-dimensional structures are observed for different amplitudes of the primary TS wave. For branch-II TS-wave amplitudes A_{II} greater than 0.6% (non-dimensionalized by the local edge velocity), 'K-type' fundamental secondary modes are observed. For amplitudes $0.3\% < A_{II} < 0.6\%$, 'H-type' subharmonic modes are observed (i.e. the secondary modes are subharmonics of the TS wave). Subharmonic modes of 'C-type' (having a specific spanwise wavenumber β_c) are

observed for $A_{II} \approx 0.3\%$. Finally, if $A_{II} < 0.2\%$ the TS wave decays without significant excitation of three-dimensional modes.

The observations for low amplitudes ($A_{II} < 0.6\%$) can be explained in the context of the secondary-instability theory of Herbert (1983, 1988). For a given frequency and Reynolds number, the growth rates for secondary modes depend on the primary-wave amplitude. Beyond a critical amplitude, the first modes to be excited are subharmonic modes with wavenumbers $\beta \approx \beta_c$. As the TS-wave amplitude is increased, the most unstable wavenumber increases ($\beta > \beta_c$) consistent with the observations. The dominance of the fundamental mode in the experiments for $A_{II} > 0.6\%$, however, is not fully explained by the secondary-instability theory. While the growth rates of fundamental modes increase more rapidly with A than do the subharmonic growth rates, they remain smaller for TS-wave amplitudes less than approximately 3% (Herbert 1988). Thus the bias towards fundamental modes for larger TS-wave amplitudes is likely the result of differences in the receptivity. Herbert (1988) has suggested that streamwise vorticity in wind tunnels could lead to such a bias. The simulations of Singer, Reed & Ferziger (1989) for channel flow demonstrate the significant role of streamwise vorticity in the development of fundamental modes. The dominant secondary instability switched from subharmonic to fundamental when longitudinal vortices were added to the initial conditions.

The experiments of Kachanov & Levchenko (1984) are another example where significant variations in the transition behaviour resulted from different initial amplitudes for the two-dimensional primary wave. This behaviour was also seen in the analysis of Crouch & Herbert (1993) which is based on the nonlinear interaction of the primary and secondary modes; comparisons between the analysis and the experiments show good agreement. For small primary-wave amplitudes, no secondary instability is excited and the primary wave decays downstream of branch II. For moderate primary-wave amplitudes, the secondary instability grows but has a weak nonlinear interaction with the primary wave, and both waves ultimately decay without triggering transition. At larger primary-wave amplitudes, the secondary mode grows rapidly leading to a strong nonlinear interaction with the primary mode resulting in transition.

Focusing on the amplitudes required for sustained growth after the nonlinear interaction of the primary and secondary modes, Herbert & Crouch (1990) calculated threshold amplitudes for transition. The thresholds define minimum initial-amplitude levels required for these modes to cause transition. For this simplified scenario of transition due a given set of primary and secondary modes, only the initial amplitudes are required to predict the occurrence and location of transition. There have been a number of receptivity analyses dealing with the excitation of two-dimensional primary-instability modes. The analyses have made use of large-Reynolds-number asymptotic methods and generalizations of the Orr–Sommerfeld equation. For a detailed discussion, see the reviews of Goldstein & Hultgren (1989), Kerschen (1989), Crouch (1994), Choudhari & Streett (1994), and Saric, Reed & Kerschen (1994). There have also been a few studies on the excitation of three-dimensional TS waves. Choudhari & Kerschen (1990) and Tadjfar & Bodonyi (1992) considered the localized receptivity resulting from three-dimensional roughness or suction using asymptotic methods. Crouch & Bertolotti (1992) considered the non-localized receptivity to TS waves due to surface waviness using a generalization of the Orr–Sommerfeld equation and the parabolized stability equations. In general, the amplitudes of these three-dimensional TS waves cannot be related to the required amplitudes for the secondary instabilities. There is a potential for the Orr–Sommerfeld and Squire modes to feed the secondary

instability, but for most wavenumbers of interest these modes experience significant decay prior to the onset of secondary instability. (A notable exception is the interaction of an unstable TS wave with a weakly decaying longitudinal vortex leading to K-type secondary modes.) Other studies have shown that the strongest effective receptivity for primary modes occurs in the neighbourhood of their lower-branch neutral points. In the neighbourhood of the secondary-mode neutral point, the parametric forcing is already established – thus triggering the growth of the secondary modes and also altering the receptivity characteristics. For these conditions, special consideration is needed to determine the initial secondary-instability amplitudes.

The analysis of secondary-instability receptivity requires the proper inclusion of the two-dimensional primary instability. The finite-amplitude TS wave influences the receptivity to three-dimensional disturbances through two different mechanisms. First, the TS wave provides a parametric forcing through an alteration of the linear operator governing the three-dimensional instability. Thus the TS wave leads to a modification of the eigenmodes that are to be excited during the receptivity process. The eigenmodes resulting from the Floquet analysis are generally quite distinct from the eigenmodes associated with three-dimensional primary instabilities. For example, the secondary instability occurs over a broad band of spanwise wavenumbers. For a fixed frequency and Reynolds number, the unstable-mode bandwidth increases with increasing primary-wave amplitude. In the absence of the parametric forcing, however, much of the wavenumber spectrum is strongly damped. The disturbance velocity profiles also differ significantly between primary and secondary modes of instability. These distinct features of the secondary modes make it difficult to infer information about the receptivity of secondary modes from a receptivity analysis of three-dimensional primary instabilities. The second mechanism by which the TS wave influences the receptivity is through direct scattering. The TS wave provides a finite-wavelength unsteady source that can scatter sound waves or be scattered by roughness or suction. Thus the TS wave can directly contribute to the receptivity.

Some of the specific issues related to the receptivity of secondary instabilities are considered in the works of Bertolotti & Crouch (1992) and Ustinov (1995). Bertolotti & Crouch considered the non-localized receptivity to two- and three-dimensional disturbances over a wavy wall by integrating the parabolized stability equations. The free stream contained both a fundamental and a subharmonic acoustic wave, allowing for the excitation of both modes of secondary instability. However, no details about the secondary-mode receptivity were obtained since the work focused on relating the transition onset to the waviness amplitude without decoupling the receptivity and instability growth. This decoupling is required for the non-localized receptivity since the excitation and growth of disturbances both occur over an extended streamwise distance (Crouch 1992*a*). Another complication associated with the non-localized problem is the influence of the initial upstream amplitude of streamwise vortices. The study of Bertolotti & Crouch demonstrates the importance of quantifying the receptivity to secondary instabilities since the three-dimensional modes are often initiated in the presence of parametric forcing. Ustinov (1995) considered the excitation of fundamental secondary instabilities in channel flow. The fundamental modes are excited directly by the scattering of the primary TS wave, without the need for acoustic modulation. This leads to a more simplified analysis compared to the subharmonic receptivity. In the context of the current work, the fundamental-mode receptivity results from a lower-order interaction as compared to the subharmonic mode. Because the fundamental mode is excited at lower order, the receptivity provides a potential bias toward fundamental modes as pointed out by Ustinov. However, the channel-

flow analysis of Ustinov did not consider the relative strengths of fundamental- and subharmonic-mode receptivity.

In this paper, we consider the localized receptivity to fundamental and subharmonic secondary instabilities in boundary layers. The velocity is expanded in terms of small perturbations characterizing an acoustic free-stream disturbance and a surface variation due to local roughness or suction. The TS wave is considered to be part of the basic flow leading to a non-homogeneous set of secondary-instability equations. These equations contain periodic coefficients due to the presence of the TS wave. Solution of these equations yields the receptivity over a wide range of parameters consistent with the stability analysis of Herbert (1988). Fundamental modes are excited directly by the surface variation as discussed in §3. The analysis leads to a simple measure for the receptivity of fundamental modes which is independent of the surface-variation shape. The excitation of subharmonic modes involves the interaction of an acoustic wave with the surface-generated disturbance; this analysis is presented in §4. For subharmonic modes, the analysis leads to a measure for the receptivity which is surface-variation independent only for symmetric variation shapes. Results for both fundamental and subharmonic modes are presented in §5, including a discussion on their relative importance for transition. Section 6 presents some conclusions. The analysis, results and discussion focus on describing the basic mechanisms and on characterizing their potential relevance for causing transition.

2. Formulation

We consider the local excitation of three-dimensional disturbances in a flat-plate boundary layer in the presence of a finite-amplitude two-dimensional TS wave. The three-dimensional disturbances are at the fundamental and subharmonic frequencies of the initial TS wave and can be related directly to secondary instabilities. Excitation of the fundamental modes results from the scattering of the TS wave by surface roughness or suction. Subharmonic modes are excited through the interaction of an acoustic wave at the subharmonic frequency, steady surface-generated disturbances containing the appropriate streamwise and spanwise variation, and the TS wave. Boundary layer velocities (u, v, w) correspond to the streamwise x, surface-normal y, and spanwise z directions, respectively. All quantities are non-dimensionalized using the free-stream velocity U_∞ and the reference length $\delta_r = (\nu x^*/U_\infty)^{1/2}$, where x^* is the streamwise position of the surface variation. This introduces the Reynolds number $R = U_\infty \delta_r/\nu$ based on the kinematic viscosity ν.

The flow is governed by the three-dimensional incompressible Navier–Stokes equations. Taking the curl of the momentum equation and using continuity removes the explicit dependence on pressure yielding the vorticity transport equation. These are three scalar equations for the vorticity components which can be related to the velocity through the conditions $\nabla \times \boldsymbol{v} = \Omega = (\xi, \eta, \zeta)$. Taking $\partial/\partial x$ of the ζ-vorticity equation and subtracting $\partial/\partial z$ of the ξ-vorticity equation leads to the generalized Orr–Sommerfeld equation:

$$\mathrm{M}_{OS}[\boldsymbol{v}] + \mathrm{N}_{OS}[\boldsymbol{v}, \boldsymbol{v}] = 0, \tag{2.1a}$$

$$\mathrm{M}_{OS}[\boldsymbol{v}] = \left(\frac{1}{R}\nabla^2 - \frac{\partial}{\partial t}\right)\nabla^2 v, \tag{2.1b}$$

$$\mathrm{N}_{OS}[\boldsymbol{v}, \boldsymbol{v}] = -\frac{\partial}{\partial x}(\boldsymbol{v}\cdot\nabla)\zeta + \frac{\partial}{\partial x}(\Omega\cdot\nabla)w + \frac{\partial}{\partial z}(\boldsymbol{v}\cdot\nabla)\xi - \frac{\partial}{\partial z}(\Omega\cdot\nabla)u. \tag{2.1c}$$

Taking $\partial/\partial z$ of the η-vorticity equation leads to the generalized Squire's equation:

$$\mathrm{M}_{SQ}[\boldsymbol{v}] + \mathrm{N}_{SQ}[\boldsymbol{v}, \boldsymbol{v}] = 0, \tag{2.2a}$$

$$\mathrm{M}_{SQ}[\boldsymbol{v}] = \left(\frac{1}{R}\nabla^2 - \frac{\partial}{\partial t}\right)\frac{\partial \eta}{\partial z}, \tag{2.2b}$$

$$\mathrm{N}_{SQ}[\boldsymbol{v}, \boldsymbol{v}] = -\frac{\partial}{\partial z}(\boldsymbol{v}\cdot\nabla)\eta + \frac{\partial}{\partial z}(\Omega\cdot\nabla)v. \tag{2.2c}$$

In the incompressible limit, an acoustic free-stream disturbance at the subharmonic frequency, $\hat{\omega} = \omega/2$, leads to the boundary condition

$$u \to 1 + \epsilon\cos\hat{\omega}t \quad \text{as} \quad y \to \infty. \tag{2.3}$$

The small parameter ϵ represents the acoustic amplitude. Surface roughness leads to the boundary condition

$$u = v = w = 0 \quad \text{at} \quad y = \delta H(x)\mathrm{e}^{\mathrm{i}\beta z}, \tag{2.4}$$

and surface suction is represented by the condition

$$u = w = 0, \quad v = -\delta H(x)\mathrm{e}^{\mathrm{i}\beta z} \quad \text{at} \quad y = 0. \tag{2.5}$$

The small parameter δ corresponds to a non-dimensional roughness height in (2.4) and a non-dimensional suction velocity in (2.5).

We first separate the velocity into a prescribed base flow consisting of the Blasius profile and the TS wave, and an unknown three-dimensional disturbance

$$\boldsymbol{v}(x, y, z, t) = \boldsymbol{v}_0(y) + A\boldsymbol{v}_1(x, y, t) + \boldsymbol{v}_3(x, y, z, t). \tag{2.6}$$

The Blasius flow $\boldsymbol{v}_0$ is subject to the quasi-parallel approximation which neglects the slow streamwise divergence of the boundary layer. This approximation is justified by the short streamwise distance over which the receptivity occurs and by the condition that δ is small. Crouch & Spalart (1995) show that the analysis for the receptivity to TS waves, following this approximation, is in good agreement with direct numerical simulations. The TS wave has the form

$$\boldsymbol{v}_1(x, y, t) = \boldsymbol{v}_{TS}(y)\mathrm{e}^{\mathrm{i}(\alpha x - \omega t)} + \boldsymbol{v}^{\dagger}_{TS}(y)\mathrm{e}^{-\mathrm{i}(\alpha x - \omega t)} \tag{2.7}$$

where $\dagger$ represents the complex conjugate. The amplitude A is defined as the maximum r.m.s. of the TS-wave streamwise-velocity fluctuation. The r.m.s. level is used to be consistent with earlier stability analyses. Substituting (2.6) into (2.1*a*) and (2.2*a*) and defining new linear operators $\mathrm{L}[\boldsymbol{v}] = \mathrm{M}[\boldsymbol{v}] + \mathrm{N}[\boldsymbol{v}, \boldsymbol{v}_0] + \mathrm{N}[\boldsymbol{v}_0, \boldsymbol{v}]$ and $\mathrm{P}[\boldsymbol{v}] = \mathrm{N}[\boldsymbol{v}, \boldsymbol{v}_1] + \mathrm{N}[\boldsymbol{v}_1, \boldsymbol{v}]$ yields

$$\mathrm{L}_{OS}[\boldsymbol{v}_3] + A\mathrm{P}_{OS}[\boldsymbol{v}_3] = -\mathrm{N}_{OS}[\boldsymbol{v}_3, \boldsymbol{v}_3], \tag{2.8}$$

$$\mathrm{L}_{SQ}[\boldsymbol{v}_3] + A\mathrm{P}_{SQ}[\boldsymbol{v}_3] = -\mathrm{N}_{SQ}[\boldsymbol{v}_3, \boldsymbol{v}_3]. \tag{2.9}$$

Neglecting the right-hand-side terms of (2.8) and (2.9) and imposing homogeneous boundary conditions yields the linear secondary-instability equations considered by Herbert (1988). In order to apply the Floquet theory, the small-amplitude variation of the TS wave is neglected over the region of receptivity (i.e. we consider $\alpha_i = 0$). Although this condition is only strictly satisified at the TS-wave neutral points, results from the stability theory support its application over the full streamwise region of interests. By introducing a coordinate transformation $X = x - ct$, where c is the

phase speed of the TS wave, the temporal dependence of the operators P_{OS} and P_{SQ} is removed. The coefficients of these operators are then periodic in the variable X. Following Floquet theory (Herbert & Bertolotti 1985), the solution to the linear stability equations can be written as

$$B\mathrm{e}^{\sigma t}\mathrm{e}^{\gamma X}\mathrm{e}^{\mathrm{i}\beta z}\sum_{n=-\infty}^{\infty}\boldsymbol{v}_n(y)\mathrm{e}^{\mathrm{i}n\hat{\alpha}X}. \tag{2.10}$$

The characteristic exponent is denoted by γ and $\hat{\alpha} = \alpha/2$. These modes can be separated into fundamental, subharmonic, and detuned modes. Here we focus on the fundamental and subharmonic modes. Separating out these modes and imposing the conditions for spatial growth, the fundamental secondary instability has the form

$$\boldsymbol{v}_F(x,y,z,t) = B_F\mathrm{e}^{\gamma x}\mathrm{e}^{\mathrm{i}\beta z}\sum_{n\ \mathrm{even}}\boldsymbol{v}_n(y)\mathrm{e}^{\mathrm{i}n(\hat{\alpha}x-\hat{\omega}t)}, \tag{2.11}$$

and the subharmonic instability has the form

$$\boldsymbol{v}_S(x,y,z,t) = B_S\mathrm{e}^{\gamma x}\mathrm{e}^{\mathrm{i}\beta z}\sum_{n\ \mathrm{odd}}\boldsymbol{v}_n(y)\mathrm{e}^{\mathrm{i}n(\hat{\alpha}x-\hat{\omega}t)}, \tag{2.12}$$

where we have imposed $\sigma = \gamma c$ for spatial growth (Herbert & Bertolotti 1985). The most unstable secondary-instability mode is tuned to the TS wave. Focusing on the most unstable mode, γ and the entire coefficient of $\exp(\mathrm{i}\beta z)$ in (2.11) and (2.12) are real (Herbert 1984). The relative magnitudes of the functions $\boldsymbol{v}_n$ are fixed by the eigensolution, each being scaled by the amplitude B.

3. Analysis for fundamental secondary instabilities

For the excitation of fundamental modes, we seek a solution of (2.1*a*)–(2.5) of the form of (2.6) with

$$\boldsymbol{v}_3(x,y,z,t) = \delta\boldsymbol{v}_\delta(x,y,z,t). \tag{3.1}$$

A homogeneous free-stream boundary condition is applied since the subharmonic acoustic wave does not directly couple with the fundamental mode. An $O(\epsilon)$ acoustic wave at the fundamental frequency could also excite the fundamental mode, similar to the subharmonic excitation discussed in §4. However, this would occur at higher order (i.e at $O(\epsilon\delta)$) and is likely to be a weaker mechanism for typical values of ϵ. Substituting (3.1) into (2.8), (2.9), (2.4), and (2.5) and collecting coefficients of δ yields

$$\mathrm{L}_{OS}[\boldsymbol{v}_\delta] + A\mathrm{P}_{OS}[\boldsymbol{v}_\delta] = 0, \tag{3.2}$$

$$\mathrm{L}_{SQ}[\boldsymbol{v}_\delta] + A\mathrm{P}_{SQ}[\boldsymbol{v}_\delta] = 0, \tag{3.3}$$

$$u_\delta, v_\delta, w_\delta \to 0 \quad \text{as} \quad y \to \infty, \tag{3.4}$$

$$u_\delta = -\left(\frac{\partial u_0}{\partial y} + A\frac{\partial u_1}{\partial y}\right)H(x)\mathrm{e}^{\mathrm{i}\beta z},\ v_\delta = w_\delta = 0 \quad \text{at} \quad y = 0, \tag{3.5}$$

or

$$v_\delta = -H(x)\mathrm{e}^{\mathrm{i}\beta z},\ u_\delta = w_\delta = 0 \quad \text{at} \quad y = 0. \tag{3.6}$$

The wall boundary condition (3.5) is used for the problem of surface roughness and (3.6) is used for surface suction. We have made use of the condition $\delta \ll 1$ to move the roughness boundary condition from $y = \delta H(x)\exp(\mathrm{i}\beta z)$ to $y = 0$ via a Taylor expansion.

The surface variation produces steady and unsteady disturbance fields at $O(\delta)$. We represent the surface-variation function $H(x)$ by the Fourier integral

$$H(x) = \frac{1}{2\pi}\int_{-\infty}^{\infty} \widetilde{H}(k)\mathrm{e}^{\mathrm{i}kx}\mathrm{d}k, \tag{3.7}$$

where

$$\widetilde{H}(k) = \int_{-\infty}^{\infty} H(x)\mathrm{e}^{-\mathrm{i}kx}\mathrm{d}x. \tag{3.8}$$

The resulting velocity field can be written as

$$\boldsymbol{v}_\delta(x,y,z,t) = \mathrm{e}^{\mathrm{i}\beta z}\sum_{n\ \text{even}} \mathrm{e}^{-\mathrm{i}n\hat{\omega}t}\frac{1}{2\pi}\int_{-\infty}^{\infty}\tilde{\boldsymbol{v}}_{\delta n}(k,y)\mathrm{e}^{\mathrm{i}kx}\mathrm{d}k. \tag{3.9}$$

The steady disturbance field generated by the flow over the surface irregularity is given by $\tilde{\boldsymbol{v}}_{\delta 0}$. This is similar to the disturbance considered in earlier works (see for example Crouch 1992*b*). In addition, there are unsteady velocity components generated by the scattering of the TS wave, $\tilde{\boldsymbol{v}}_{\delta n}$, $|n| > 0$. The unsteady disturbances are characterized by the frequency $\omega = 2\hat{\omega}$, providing a direct coupling with the fundamental secondary instability.

Substituting (3.9) into (3.2)–(3.6) yields a coupled set of equations for the functions $\tilde{\boldsymbol{v}}_{\delta n}(k,y)$, n even. The equations for $\tilde{\boldsymbol{v}}_{\delta n}(k,y)$ are coupled to the equations for $\tilde{\boldsymbol{v}}_{\delta n-2}(k-2\hat{\alpha},y)$ and $\tilde{\boldsymbol{v}}_{\delta n+2}(k+2\hat{\alpha},y)$ due to the interaction with the TS wave – $\boldsymbol{v}_{TS}(y)$ and $\boldsymbol{v}^{\dagger}_{TS}(y)$, respectively. To illustrate the coupling with the surface geometry $H(x)$, we consider the roughness boundary condition (3.5) for the u_δ velocity component. Substituting for u_δ, u_1, and $H(x)$ and applying harmonic balance yields

$$\tilde{u}_{\delta 0}(k,y) = -\frac{\partial u_0}{\partial y}\widetilde{H}(k), \tag{3.10a}$$

$$\tilde{u}_{\delta 2}(k+2\hat{\alpha},y) = -A\frac{\partial u_{TS}}{\partial y}\widetilde{H}(k), \tag{3.10b}$$

$$\tilde{u}_{\delta -2}(k-2\hat{\alpha},y) = -A\frac{\partial u^{\dagger}_{TS}}{\partial y}\widetilde{H}(k), \tag{3.10c}$$

$$\tilde{u}_{\delta n}(k+n\hat{\alpha},y) = 0, |n| > 2 \quad \text{at} \quad y = 0. \tag{3.10d}$$

For the coupled set of velocity functions, the transform of the surface-geometry function appears in the boundary condition evaluated at a single wavenumber. Solution of the non-homogeneous equations (3.2)–(3.6) yields the functions $\tilde{\boldsymbol{v}}_{\delta n}(k+n\hat{\alpha},y)$ for a given value of k as prescribed by the boundary conditions.

Considering only a few terms of the summation on n, (3.9) can be rewritten as

$$\begin{aligned}\boldsymbol{v}_\delta(x,y,z,t) = \mathrm{e}^{\mathrm{i}\beta z}\frac{1}{2\pi}\int_{-\infty}^{\infty}\big(\cdots &+ \tilde{\boldsymbol{v}}_{\delta -2}(k-2\hat{\alpha},y)\mathrm{e}^{\mathrm{i}(k-2\hat{\alpha})x+\mathrm{i}2\hat{\omega}t}\\ &+\tilde{\boldsymbol{v}}_{\delta 0}(k,y)\mathrm{e}^{\mathrm{i}kx} + \tilde{\boldsymbol{v}}_{\delta +2}(k+2\hat{\alpha},y)\mathrm{e}^{\mathrm{i}(k+2\hat{\alpha})x-\mathrm{i}2\hat{\omega}t}+\cdots\big)\,\mathrm{d}k.\end{aligned} \tag{3.11}$$

This integral is evaluated using contour integration. The integration contours can be closed in the upper half-plane since we are interested in the disturbance downstream of its source, $x > 0$. Sufficiently far from the source, the total disturbance will be dominated by the least-stable secondary-instability eigenmode. The contribution to this eigenmode is given by $2\pi\mathrm{i}$ times the residues at the poles $n\hat{\alpha}-\mathrm{i}\gamma$ (n even) when $k = -\mathrm{i}\gamma$:

$$\boldsymbol{v}_f(x,y,z,t) = \mathrm{i}\mathrm{e}^{\mathrm{i}\beta z}\sum_{n\ \text{even}} \mathrm{e}^{-\mathrm{i}n\hat{\omega}t}\tilde{\boldsymbol{v}}_{\delta n}(n\hat{\alpha}-\mathrm{i}\gamma,y)\mathrm{e}^{\mathrm{i}(n\hat{\alpha}-\mathrm{i}\gamma)x}. \tag{3.12}$$

When $\gamma > 0$, the poles lie in the lower half-plane and causality requires that the inversion contour pass below these poles. Note that the functions $\tilde{\boldsymbol{v}}_{\delta n}(n\hat{\alpha} - \mathrm{i}\gamma, y)$, for different values of n, are related since they correspond to a single eigenfunction as given by (2.11) (the amplitude B_F multiplies the entire Fourier series). Therefore, it is sufficient to evaluate the residue associated with the function $\tilde{\boldsymbol{v}}_{\delta 2}(2\hat{\alpha} - \mathrm{i}\gamma, y)$ in order to determine the instability amplitude. The functions for $n < 0$ are complex conjugates of the functions for $n > 0$. The results presented in §5 are based on low-order truncations of the Fourier series.

Introducing a measure for the fundamental-mode response residue

$$K_F = 2\tilde{u}_{\delta 2}(2\hat{\alpha} - \mathrm{i}\gamma, y_{max})/\widetilde{H}(-\mathrm{i}\gamma), \tag{3.13}$$

where y_{max} is the location of maximum disturbance magnitude and noting that $\boldsymbol{v}_F = \delta \boldsymbol{v}_f$, the fundamental secondary-instability amplitude can be written as

$$B_F = \delta |K_F \widetilde{H}(-\mathrm{i}\gamma)|. \tag{3.14}$$

The value of K_F provides a measure of the receptivity, independent of the shape of the surface variation. $\widetilde{H}(-\mathrm{i}\gamma)$ is the Fourier transform of $H(x)$ evaluated at the complex wavenumber associated with the steady component ($n = 0$) of the fundamental mode. The amplitude B_F provides the secondary-instability response which can be used to make estimations about transition. Note that B_F is defined as a magnitude for a given Fourier component, while the TS-wave amplitude A is defined as an r.m.s. level.

4. Analysis for subharmonic secondary instabilities

The excitation of subharmonic secondary instabilities requires a higher-order interaction than the fundamental modes. We seek a solution of (2.1*a*)–(2.5) of the form of (2.6) with

$$\boldsymbol{v}_3(x, y, z, t) = \epsilon \boldsymbol{v}_\epsilon(x, y, t) + \delta \boldsymbol{v}_\delta(x, y, z, t) + \epsilon\delta \boldsymbol{v}_{\epsilon\delta}(x, y, z, t). \tag{4.1}$$

This expansion is similar to those considered for receptivity to TS waves. The $O(\epsilon)$ disturbance is generated by the acoustic wave and the $O(\delta)$ disturbance is the result of the surface variation. The interaction of the acoustic and surface-generated disturbances at $O(\epsilon\delta)$ then produces an unsteady disturbance with length and time scales that may match those of the three-dimensional boundary-layer instabilities. Unlike expansions considered for TS waves, the $O(\epsilon)$ function depends on x and the $O(\delta)$ function depends on t. The $O(\epsilon^2)$ and $O(\delta^2)$ disturbances are not included in (4.1) since their contributions to the receptivity occur at higher order; this can be verified by harmonic balance.

Substituting (4.1) into (2.8), (2.9), and (2.3)–(2.5) and collecting coefficients of like powers in ϵ and δ yields

Order ϵ:

$$\mathrm{L}_{OS}[\boldsymbol{v}_\epsilon] + A\mathrm{P}_{OS}[\boldsymbol{v}_\epsilon] = 0, \tag{4.2}$$

$$\mathrm{L}_{SQ}[\boldsymbol{v}_\epsilon] + A\mathrm{P}_{SQ}[\boldsymbol{v}_\epsilon] = 0, \tag{4.3}$$

$$u_\epsilon \to 1/2(\mathrm{e}^{\mathrm{i}\hat{\omega}t} + \mathrm{e}^{-\mathrm{i}\hat{\omega}t}), v_\epsilon, w_\epsilon \to 0 \quad \text{as} \quad y \to \infty, \tag{4.4}$$

$$u_\epsilon = v_\epsilon = w_\epsilon = 0 \quad \text{at} \quad y = 0; \tag{4.5}$$

Order δ:

$$\mathrm{L}_{OS}[\boldsymbol{v}_\delta] + A\mathrm{P}_{OS}[\boldsymbol{v}_\delta] = 0, \tag{4.6}$$

$$\mathrm{L}_{SQ}[\boldsymbol{v}_\delta] + A\mathrm{P}_{SQ}[\boldsymbol{v}_\delta] = 0, \tag{4.7}$$

$$u_\delta, v_\delta, w_\delta \to 0 \quad \text{as} \quad y \to \infty, \tag{4.8}$$

$$u_\delta = -\left(\frac{\partial u_0}{\partial y} + A\frac{\partial u_1}{\partial y}\right) H(x)\mathrm{e}^{\mathrm{i}\beta z}, \; v_\delta = w_\delta = 0 \quad \text{at} \quad y = 0, \tag{4.9}$$

or

$$v_\delta = -H(x)\mathrm{e}^{\mathrm{i}\beta z}, \; u_\delta = w_\delta = 0 \quad \text{at} \quad y = 0; \tag{4.10}$$

Order $\epsilon\delta$:

$$\mathrm{L}_{OS}[\boldsymbol{v}_{\epsilon\delta}] + A\mathrm{P}_{OS}[\boldsymbol{v}_{\epsilon\delta}] = -\mathrm{N}_{OS}[\boldsymbol{v}_\epsilon, \boldsymbol{v}_\delta] - \mathrm{N}_{OS}[\boldsymbol{v}_\delta, \boldsymbol{v}_\epsilon], \tag{4.11}$$

$$\mathrm{L}_{SQ}[\boldsymbol{v}_{\epsilon\delta}] + A\mathrm{P}_{SQ}[\boldsymbol{v}_{\epsilon\delta}] = -\mathrm{N}_{SQ}[\boldsymbol{v}_\epsilon, \boldsymbol{v}_\delta] - \mathrm{N}_{SQ}[\boldsymbol{v}_\delta, \boldsymbol{v}_\epsilon], \tag{4.12}$$

$$u_{\epsilon\delta}, v_{\epsilon\delta}, w_{\epsilon\delta} \to 0 \quad \text{as} \quad y \to \infty, \tag{4.13}$$

$$u_{\epsilon\delta} = -\left(\frac{\partial u_\epsilon}{\partial y}\right) H(x)\mathrm{e}^{\mathrm{i}\beta z},$$

$$v_{\epsilon\delta} = -\left(\frac{\partial v_\epsilon}{\partial y}\right) H(x)\mathrm{e}^{\mathrm{i}\beta z}, \; w_{\epsilon\delta} = 0 \quad \text{at} \quad y = 0, \tag{4.14}$$

or

$$u_{\epsilon\delta} = v_{\epsilon\delta} = w_{\epsilon\delta} = 0 \quad \text{at} \quad y = 0. \tag{4.15}$$

The wall boundary conditions (4.9) and (4.15) are used for the problem of surface roughness, (4.10) and (4.15) are used for surface suction. We have made use of the condition $\delta \ll 1$ to move the roughness boundary condition from $y = \delta H(x)\exp(\mathrm{i}\beta z)$ to $y = 0$. In the limit of $A = 0$, (4.2)–(4.15) reduce to the localized receptivity equations for TS waves considered by Crouch (1992*b*).

The $O(\epsilon)$ flow is decoupled from the disturbance generated by the surface variation. This component of velocity represents the Stokes flow induced by the acoustic wave of frequency $\hat{\omega}$ in the presence of the TS wave and can be written in the form

$$\boldsymbol{v}_\epsilon(x, y, t) = \sum_{l \text{ even}} \left(\boldsymbol{v}_{\epsilon l}(y)\mathrm{e}^{\mathrm{i}l\hat{\alpha}x}\mathrm{e}^{-\mathrm{i}(l+1)\hat{\omega}t} + \text{c.c}\right), \tag{4.16}$$

where c.c. signifies complex conjugate. In the travelling frame, this forced velocity has the form of (2.10) with $\gamma = \beta = 0$ and a detuning of $\sigma_i = -\hat{\omega}$. The detuning requires the inclusion of the complex conjugate in order for the velocity to be real. The components with $l = 0$ form the Stokes wave and the components with $l \pm 2$ are $O(\epsilon A)$ disturbances generated due to the direct interaction of the Stokes wave and the TS wave. The magnitude and phase of the profiles are set by the condition $u_{\epsilon 0} \to 1/2$ as $y \to \infty$.

The surface variation produces steady and unsteady disturbance fields at $O(\delta)$. We represent the surface-variation function $H(x)$ by the Fourier integral (3.7). The resulting velocity field can be written as

$$\boldsymbol{v}_\delta(x, y, z, t) = \mathrm{e}^{\mathrm{i}\beta z} \sum_{m \text{ odd}} \mathrm{e}^{-\mathrm{i}(m-1)\hat{\omega}t} \frac{1}{2\pi} \int_{-\infty}^{\infty} \tilde{\boldsymbol{v}}_{\delta m}(k, y)\mathrm{e}^{\mathrm{i}kx}\mathrm{d}k. \tag{4.17}$$

The use of m odd, in contrast to (3.9), is motivated by the form of the subharmonic modes (2.12) which are considered at $O(\epsilon\delta)$. The steady disturbance field generated by the flow over the surface irregularity is given by $\tilde{\boldsymbol{v}}_{\delta 1}$. This is similar to the steady disturbance considered in (3.9). The unsteady velocity components generated by the scattering of the TS wave are given by $\tilde{\boldsymbol{v}}_{\delta m}$, $|m - 1| > 0$. The unsteady disturbances are characterized by the frequency $\omega = 2\hat{\omega}$ and its superharmonics. Therefore,

these unsteady disturbances do not directly couple with the subharmonic secondary instabilities.

In order to determine the form for the $O(\epsilon\delta)$ velocity, we consider a single term on the right-hand side of (4.11). This can be represented by the scalar product $f_\epsilon g_\delta$, where f and g are velocities, or derivatives of velocities, corresponding to (4.16) and (4.17), respectively. Using (4.16) and (4.17), the scalar product is given by

$$\begin{aligned} f_\epsilon(x,y,t)\ g_\delta(x,y,z,t) \\ = \mathrm{e}^{\mathrm{i}\beta z} \sum_{n\ \mathrm{odd}} \mathrm{e}^{-\mathrm{i}n\hat{\omega}t} \sum_{m\ \mathrm{odd}} \left(\frac{1}{2\pi} \int_{-\infty}^{\infty} f_{\epsilon n-m}(y) \tilde{g}_{\delta m}(k+(m-n)\hat{\alpha}, y) \mathrm{e}^{\mathrm{i}kx} \mathrm{d}k \right. \\ \left. + \frac{1}{2\pi} \int_{-\infty}^{\infty} f^{\dagger}_{\epsilon m-n-2}(y) \tilde{g}_{\delta m}(k+(m-n-2)\hat{\alpha}, y) \mathrm{e}^{\mathrm{i}kx} \mathrm{d}k \right). \end{aligned} \tag{4.18}$$

The resulting velocity field can be written as

$$\boldsymbol{v}_{\epsilon\delta}(x,y,z,t) = \mathrm{e}^{\mathrm{i}\beta z} \sum_{n\ \mathrm{odd}} \mathrm{e}^{-\mathrm{i}n\hat{\omega}t} \frac{1}{2\pi} \int_{-\infty}^{\infty} \tilde{\boldsymbol{v}}_{\epsilon\delta n}(k,y) \mathrm{e}^{\mathrm{i}kx} \mathrm{d}k. \tag{4.19}$$

Each value of n represents a different frequency and the corresponding velocity fields are given by Fourier integrals. Note that the velocities for the different n are coupled through the periodic operators of (4.11) and (4.12).

The surface geometry is coupled to the $O(\epsilon\delta)$ function through the right-hand sides of (4.11) and (4.12) and, for roughness, through the boundary condition (4.15). Following the discussion in §3, we consider the $\tilde{u}_{\epsilon\delta}$ boundary condition. Substituting for $u_{\epsilon\delta}$, u_ϵ, and $H(x)$ and applying harmonic balance yields

$$\begin{aligned} \tilde{u}_{\epsilon\delta n}(k,y) = -\frac{\partial u_{\epsilon n-1}}{\partial y} \widetilde{H}(k-n\hat{\alpha}+\hat{\alpha}) \\ -\frac{\partial u^{\dagger}_{\epsilon-n-1}}{\partial y} \widetilde{H}(k-n\hat{\alpha}-\hat{\alpha}) \quad \text{at} \quad y=0. \end{aligned} \tag{4.20}$$

The function $\tilde{u}_{\epsilon\delta 1}(k,y)$ is coupled to the functions $\tilde{u}_{\epsilon\delta n}$, $n \neq 1$, evaluated at different values of the wavenumber. Considering each function evaluated at the appropriate wavenumber for coupling, (4.20) becomes

$$\begin{aligned} \tilde{u}_{\epsilon\delta n}(k+(n-1)\hat{\alpha}, y) = -\frac{\partial u_{\epsilon n-1}}{\partial y} \widetilde{H}(k) \\ -\frac{\partial u^{\dagger}_{\epsilon-(n-1)-2}}{\partial y} \widetilde{H}(k-2\hat{\alpha}) \quad \text{at} \quad y=0. \end{aligned} \tag{4.21}$$

For a given value of k, $\widetilde{H}(k)$ appears in the boundary conditions evaluated at two different wavenumbers. Consideration of the right-hand sides of (4.11) and (4.12) yields a similar result.

After determining the functions $\tilde{\boldsymbol{v}}_{\epsilon\delta n}(k,y)$ for a given $\widetilde{H}(k)$, the integral (4.19) can be evaluated similar to (3.9). Downstream of the source, the subharmonic disturbance is dominated by the least-stable eigenmode corresponding to the poles at $n\hat{\alpha} - \mathrm{i}\gamma$ (n odd)

$$\boldsymbol{v}_s(x,y,z,t) = \mathrm{i}\mathrm{e}^{\mathrm{i}\beta z} \sum_{n\ \mathrm{odd}} \mathrm{e}^{-\mathrm{i}n\hat{\omega}t} \tilde{\boldsymbol{v}}_{\epsilon\delta n}(n\hat{\alpha} - \mathrm{i}\gamma, y) \mathrm{e}^{\mathrm{i}(n\hat{\alpha}-\mathrm{i}\gamma)x}. \tag{4.22}$$

The resides at different values of n are coupled through the eigenfunction (2.12) and the functions for $n < 0$ are complex conjugates of the functions for $n > 0$.

For symmetric surface perturbations, $\widetilde{H}(-\hat{\alpha}-\mathrm{i}\gamma) = \widetilde{H}^{\dagger}(\hat{\alpha}-\mathrm{i}\gamma)$ and a simple measure for the subharmonic-mode receptivity can be evaluated. If the scattering due to the TS wave is neglected ($N = 1$ as discussed in §5.1), noting that $\boldsymbol{v}_S = \epsilon\delta\boldsymbol{v}_s$ the subharmonic-instability amplitude can be written as

$$B_S = \epsilon\delta|K_S\widetilde{H}(\hat{\alpha} - \mathrm{i}\gamma)|. \tag{4.23}$$

The value of K_S is given by

$$K_S = 2\tilde{u}_{\epsilon\delta 1}(\hat{\alpha} - \mathrm{i}\gamma, y_{max})/\widetilde{H}(\hat{\alpha} - \mathrm{i}\gamma), \tag{4.24}$$

where y_{max} is the location of maximum disturbance magnitude. This value of K_S provides a measure of the receptivity, independent of the surface variation shape (except for the assumption of symmetry). $\widetilde{H}(\hat{\alpha} - \mathrm{i}\gamma)$ is the Fourier transform of $H(x)$ evaluated at the complex wavenumber associated with the subharmonic mode ($n = 1$) of the secondary instability. The amplitude B_S provides the secondary-instability response over the full range of spanwise wavenumbers and TS-wave amplitudes covered by the Floquet theory.

At the subharmonic-mode neutral point, $\gamma \equiv 0$ and the assumption of a symmetric surface perturbation yields $\widetilde{H}(-\hat{\alpha}) = \widetilde{H}(\hat{\alpha})$. For this condition, the form for B_S given in (4.23) is also valid when the TS-wave scattering is included ($N > 1$ as considered in §5.1). Most of the results presented in §5 neglect the TS-wave scattering. To evaluate the relative strength of the TS-wave scattering compared to other secondary-instability effects, results are given for $\gamma \approx 0$.

5. Receptivity results for secondary instabilities

For a given basic flow, the secondary-instability characteristics depend on: the frequency $F = 10^6\omega\nu/U_\infty^2$, the Reynolds number R, the spanwise wavenumber $b = 10^3\beta/R$, and the TS-wave amplitude A. The excitation of subharmonic modes depends, in addition, on the relative phase between the acoustic wave and the TS wave at the source location ψ_{TS}. Since the intention of this work is to understand the basic mechanism of secondary receptivity and its potential relevance for transition, we focus our results on two frequencies $F = 124$ and $F = 56$. The frequency $F = 124$ was considered in the experiments of Kachanov & Levchenko (1984) and has since been studied extensively in the context of subharmonic secondary instabilities (see Herbert 1988). Our stability results at this frequency can easily be compared to earlier works. The two-dimensional TS wave at $F = 124$ grows from a Reynolds number of $R_I = 381$ up to $R_{II} = 606$. The frequency $F = 56$ was initially considered in the receptivity experiments of Leehey & Shapiro (1980) and meanwhile has been studied in numerous receptivity analyses. This frequency is also close to $F = 58.8$ which was considered by Klebanoff, Tidstrom & Sargent (1962) and Herbert (1985) in the context of fundamental secondary instabilities. The two-dimensional TS wave at this frequency grows from $R_I = 576$ to $R_{II} = 1105$. We focus on Reynolds numbers at, or near, branch II where the TS-wave amplitude is largest. Depending on the amplitude of the TS wave, the secondary instability can grow for a significant distance downstream of R_{II}.

Additional parameters are introduced when solving for the growth or receptivity characteristics numerically. After introducing the Fourier expansions for the disturbance velocities, the resulting governing equations are solved using a spectral collocation method. The unbounded boundary-layer domain $y \in [0, \infty)$ is first trans-

N	γ	$\lvert K_F\rvert$	$\arg(K_F)$
2	0.01008420	0.00304	5.880
4	0.01012255	0.00302	5.866
6	0.01012176	0.00302	5.866
N	γ	$\lvert K_S\rvert$	$\arg(K_S)$
1	−0.00001738	0.0790	2.555
3	−0.00000323	0.0784	2.556
5	−0.00000309	0.0784	2.556

TABLE 1. Growth rate γ and response residue K for different levels of truncation N

formed into a bounded domain $\eta \in [1, 0)$ using the algebraic mapping $\eta = \eta^*/(y+\eta^*)$, where η^* is a parameter controlling the distribution of points across the boundary layer. Odd Chebyshev polynomials are used as expansion functions that automatically satisfy homogeneous boundary conditions at infinity. This requires that we transform the boundary conditions from infinity to the wall when solving for the acoustic disturbance. The results presented are based on 30 collocation points with $\eta^* = 4.5$, which positions half of the collocation points within the displacement thickness of the boundary layer. A further increase in the resolution produces insignificant change in the results. For the conditions discussed in §5.1, an increase in the number of collocation points from 30 to 40 resulted in a 0.04% change in the growth rate and less than 0.02% change in the response residue.

5.1. *Truncation of the Fourier series*

Numerical evaluation for the stability and receptivity requires that the summations on n, in the Floquet theory, be truncated to some finite level N. For subharmonic instabilities (i.e. (2.12), (4.19), (4.22)), the lowest possible truncation is $|n| \leqslant N = 1$. This truncation includes the modes $\tilde{\boldsymbol{v}}_{\epsilon\delta-1}$ and $\tilde{\boldsymbol{v}}_{\epsilon\delta 1}$. For fundamental instabilities (i.e. (2.11), (3.9), (3.12)), the lowest truncation is $|n| \leqslant N = 2$, which includes $\tilde{\boldsymbol{v}}_{\delta-2}$, $\tilde{\boldsymbol{v}}_{\delta 0}$, and $\tilde{\boldsymbol{v}}_{\delta 2}$. Herbert, Bertolotti & Santos (1986) showed that the Fourier series converged rapidly with increased N, and that $N = 1$ and $N = 2$ are sufficient for analysing the stability of subharmonic and fundamental modes, respectively. This is further demonstrated by the spatial growth rates γ presented in table 1 for the conditions $b = 0.33$, $R = 606$, $A = 0.01$ (fundamental mode), $R = 404$, $A = 0.005$ (subharmonic mode). When N is changed from 2 to 4, the fundamental-mode growth rate changes by 4×10^{-5} (less than 0.4%). The subharmonic-mode growth rate changes by approximately 1×10^{-5} between $N = 1$ and $N = 3$.

For fundamental-mode receptivity, no significantly new physics are added when increasing the value of N. The truncation influences the receptivity primarily through changes to the eigenmode. This is in contrast to subharmonic modes where additional physics are included when increasing from $N = 1$ to $N = 3$. To be consistent with a truncation of $|n| \leqslant N$ for the $O(\epsilon\delta)$ subharmonic disturbance (4.22), the $O(\epsilon)$ acoustic disturbance (4.16) is truncated to $|n| \leqslant N - 1$, and the $O(\delta)$ surface-generated disturbance (4.17) to $|n - 1| \leqslant N - 1$. For the lowest possible subharmonic-mode truncation of $N = 1$, the acoustic disturbance is truncated to $|n| \leqslant 0$, which neglects the scattering of the acoustic wave by the TS wave. A truncation of $N = 1$ also neglects the scattering of the TS wave by the surface irregularity. The lowest subharmonic-mode truncation that includes the TS-wave scattering effects is $N = 3$.

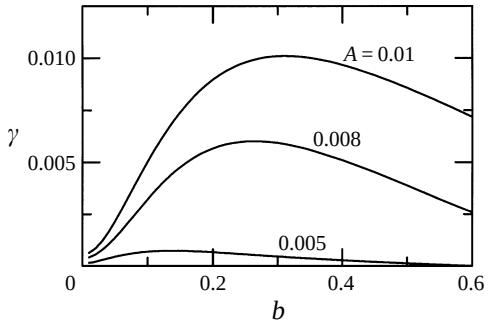

FIGURE 1. Spatial growth rates for the dominant fundamental mode at $F = 124$, $R = 606$, $A = 0.005, 0.008, 0.01$.

Table 1 shows the effects of the Fourier truncation on the response residue for both fundamental and subharmonic modes. The changes in the fundamental-mode residue are less than 1% for $N > 2$. The magnitude of the subharmonic-mode response residue also changes by less than 1% when increasing N from 1 to 3. Note that the parameters for table 1 (N odd) are chosen such that $\gamma \approx 0$ and, therefore, the results for $|K_S|$ are physically meaningful for $N > 1$. The change in the subharmonic response is a combination of the additional scattering contributions and the changes to the stability characteristics. These results demonstrate that the influence of the TS-wave scattering on the subharmonic modes is small compared to the dramatic effects of the TS-wave parametric forcing.

The results of table 1 show that truncations of $N = 2$ and $N = 1$ are sufficient for capturing dominant effects on the receptivity of fundamental and subharmonic modes, respectively. Although $N = 3$ is required to completely capture the receptivity to subharmonic secondary instabilities, a truncation of $N = 1$ provides the essential trends in the receptivity level. The results presented are based on $N = 2$ and $N = 1$. Variations of less than 1% are generally not discernible in the plotted results.

5.2. *Results for fundamental secondary instabilities*

Spatial growth rates for fundamental modes at different TS-wave amplitudes and different spanwise wavenumbers are presented in figure 1. The Reynolds number is $R = 606$ and the frequency is $F = 124$. These growth rates are in good agreement with temporal growth rates that are transformed into spatial growth using the wave speed. More detailed comparisons to earlier stability analyses are discussed in §5.3 for subharmonic modes. One of the key features of the fundamental-mode instability is the rapid drop in the growth rate as the TS-wave amplitude is decreased.

Figure 2 shows the response residue for receptivity to roughness and suction at the conditions of figure 1. The symbols correspond to the wavenumbers for maximum growth at each TS-wave amplitude. Except for the very low wavenumbers, the residue variation with wavenumber is small. The peak receptivity occurs at the intermediate TS-wave amplitude. At small amplitudes, the receptivity drops off significantly. Thus for fundamental modes, both the receptivity and growth rate are much smaller for small TS-wave amplitudes. The receptivity variation with amplitude is shown more clearly in figure 3 for a single spanwise wavenumber $b = 0.33$. The peak value occurs at $A \approx 0.0075$. The reduction in the residue for larger values of A is offset by the significant increase in the growth rate; this is not the case for smaller values of A. Thus

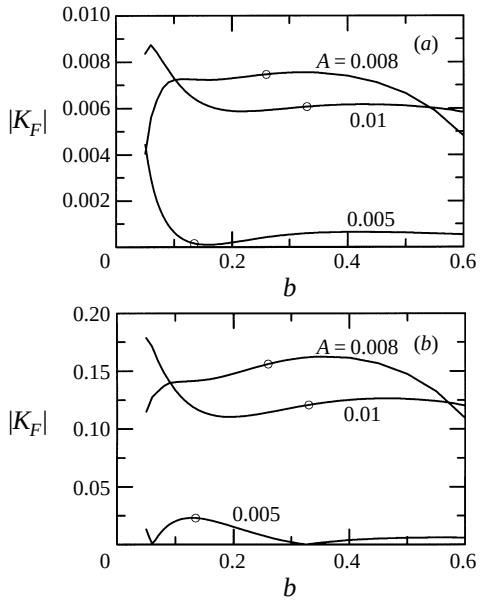

FIGURE 2. Magnitude of the response residue for fundamental-mode receptivity due to (*a*) roughness or (*b*) suction, for the conditions $F = 124$, $R = 606$, $A = 0.005$, 0.008, 0.01.

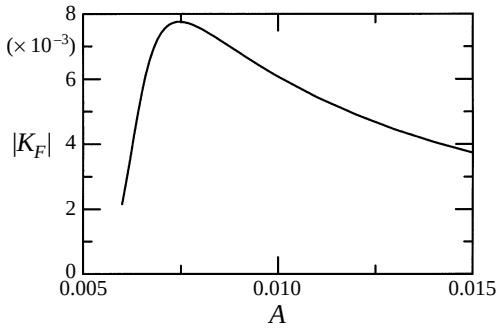

FIGURE 3. Magnitude of the response residue for fundamental-mode receptivity due to roughness, for the conditions $F = 124$, $R = 606$, $b = 0.33$.

the experimentally observed bias toward higher TS-wave amplitudes for fundamental modes is supported by the combined influence of receptivity and instability growth.

5.3. *Results for subharmonic secondary instabilities*

Before discussing the general results for subharmonic-mode receptivity, we briefly consider the spatial stability and receptivity for $A \approx 0$. Figure 4 shows the variation of the growth rate γ as a function of the primary-wave amplitude A at the Reynolds number $R = 606$. The spanwise wavenumber was chosen to satisfy Craik resonance (Craik 1971). This wavenumber has the strongest growth for small TS-wave amplitudes. The two curves are the least-stable eigenmodes predicted by the Floquet theory. Both modes are phased locked with the TS wave. At $A = 0$, the two modes collapse to an unstable three-dimensional TS wave with growth rate γ_0. Note that in general the corresponding TS wave at $A = 0$ may be damped. Results similar to figure 4 have been presented by Herbert (1983), based on temporal-stability theory.

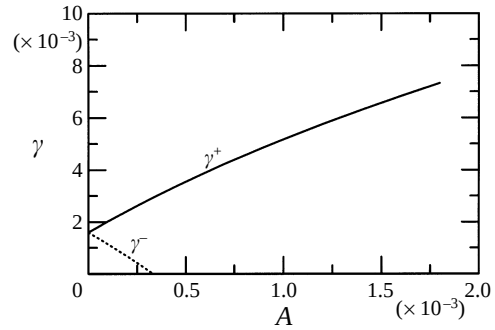

FIGURE 4. Spatial growth rates for dominant γ^+ (solid) and related γ^- (dashed) subharmonic modes at $F = 124$, $R = 606$, $b = 0.1827$.

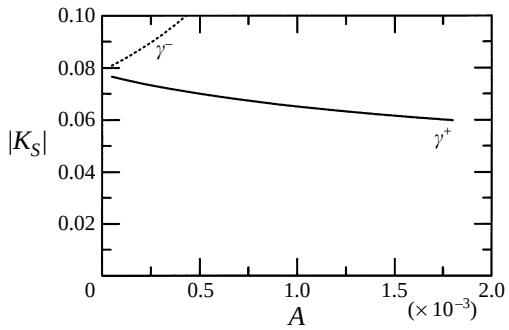

FIGURE 5. Magnitude of the response residue for dominant γ^+ (solid) and related γ^- (dashed) subharmonic modes due to roughness at $F = 124$, $R = 606$, $b = 0.1827$.

In the neighbourhood of $A = 0$, the growth rates are described by $\gamma^{\pm} \approx \gamma_0 \pm \Delta\gamma A$, where $\Delta\gamma = 4.3$ for these conditions. For $A \approx 0$, the two modes of figure 4 have comparable growth rates ($\gamma^+ \approx \gamma^-$). Therefore, both modes must be included when considering the receptivity. For larger values of A, the γ^+ mode has much stronger growth and the γ^- mode can be neglected in evaluating the response residues. The variation of the response residues $|K_S|$ for the modes $\gamma^{\pm}$ are shown in figure 5. The corresponding phases are nearly constant over this range of amplitudes, $\arg(K_S) \approx 2.9$ for γ^+ and $\arg(K_S) \approx 4.4$ for γ^-. This result is for a TS-wave phase of $\psi_{TS} = 0$; the relative magnitude of the two modes changes with different values of ψ_{TS}. The results of figure 5 show that the response residue for the dominant secondary-instability mode decreases with increasing TS-wave amplitude A. This trend is observed for both surface roughness and surface suction for all amplitudes of interest, $A \leqslant 1\%$. The rate of variation of the residue strongly depends on the phase ψ_{TS}.

Before considering the dependence of the receptivity on the spanwise wavenumber, figure 6 shows the variation of the spatial growth rate for the dominant mode at $R = 606$. Temporal growth rates for these conditions are given in Herbert (1984). A good comparison between the two results is obtained using the phase speed to transform between temporal and spatial growth. These results are also in agreement with the spatial growth rates of Herbert & Bertolotti (1985). Figure 6 shows that the maximum growth rate and the corresponding wavenumber both increase with increasing TS-wave amplitude. The response residues for localized roughness and suction are given in figure 7 for the conditions of figure 6. The range of wavenumbers

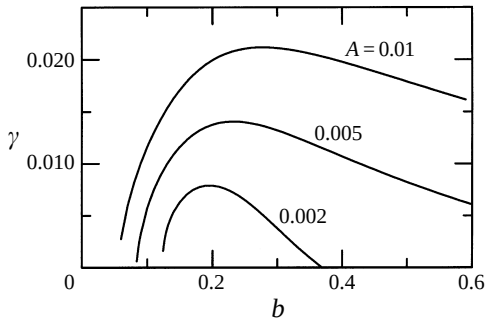

FIGURE 6. Spatial growth rates for dominant subharmonic mode at $F = 124$, $R = 606$, $A = 0.002, 0.005, 0.01$.

roughly corresponds to the range of unstable modes for these conditions. Roughness results are presented for different TS-wave amplitudes with $\psi_{TS} = 0$. The magnitude of the residue shows a general increase with increasing spanwise wavenumber. The symbols show the residue at wavenumbers for maximum growth b_{max} at the different amplitudes. At the larger amplitudes, the response residue changes very little in the neighbourhood of b_{max}. For $A = 0.2\%$, the receptivity at the higher wavenumbers $b > b_{max}$ is 2–5 times larger than at the lower wavenumbers $b < b_{max}$. This bias suggests that wavenumbers larger than b_{max} are likely to be more dominant in transition than wavenumbers smaller than b_{max} when TS-wave amplitudes are small. The response residue for localized suction is based on $\psi_{TS} = \pi$. This phase is closer to the phase for maximum localized-suction receptivity at these conditions. The response is largest for $b > b_{max}$. However, the level of variation around b_{max} is small compared to roughness receptivity and is not likely to significantly bias the initial disturbance spectrum. The relative magnitude between the response residue for roughness and suction is similar to results for receptivity to TS waves (Choudhari & Streett 1992).

The most significant parameter influencing the subharmonic-mode response residue is the TS-wave phase at the source location, ψ_{TS}. At a given Reynolds number, spanwise wavenumber, and TS-wave amplitude, there exists a phase ψ_{TS} for which the response residue goes to zero. Figure 8 shows the variation of $|K_S|$ with ψ_{TS} for different Reynolds numbers with $b = 0.33$, $A = 0.005$. The residue has one maximum and one zero (i.e. half-period) over one period of the TS wave. The maximum and zero locations depend weakly on the Reynolds number. The variation of the magnitude with Reynolds number is somewhat more significant for suction than roughness.

The influence of the phase between the acoustic wave and the TS wave can be represented explicitly by defining a maximum response residue

$$|K_S|_{max} = \max_{\psi_{TS}} |K_S|. \tag{5.1}$$

The subharmonic-mode amplitude then becomes

$$B_S = \epsilon\delta|\widetilde{H}(\hat{\alpha} - \mathrm{i}\gamma)|\ |K_S|_{max}\ \cos((\psi_{TS} - \psi_{TSmax})/2), \tag{5.2}$$

where ψ_{TSmax} corresponds to $|K_S| = |K_S|_{max}$. The value of ψ_{TSmax} depends on the frequency, the Reynolds number, the spanwise wavenumber, and the TS-wave amplitude. Figure 9 shows the variation of $|K_S|_{max}$ with Reynolds number for different values of the TS-wave amplitude. The symbols show the neutral points for the different amplitudes. For small TS-wave amplitudes, $|K_S|_{max}$ decreases with

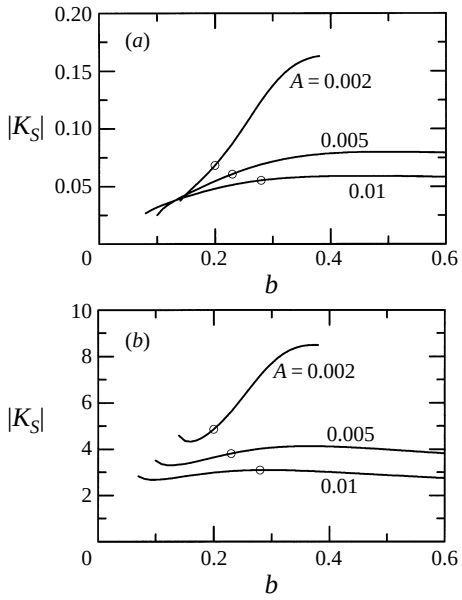

FIGURE 7. Magnitude of the response residue for subharmonic-mode receptivity due to (*a*) roughness with $\psi_{TS} = 0$, or (*b*) suction with $\psi_{TS} = \pi$, for the conditions $F = 124$, $R = 606$, $A = 0.002$, 0.005, 0.01.

increasing Reynolds number and the maximum effective receptivity occurs upstream of the neutral points. For larger TS-wave amplitudes, there is no significant variation with Reynolds number and the maximum effective receptivity will occur at the neutral points. The TS-wave amplitude does not significantly change the value of ψ_{TSmax} for larger Reynolds numbers. At $R = 600$, $\psi_{TSmax} \approx 0$ for roughness and $\psi_{TSmax} \approx 2.4$ for suction over the range of TS-wave amplitudes considered in figure 9. However, at $R = 400$ ψ_{TSmax} varied from 5.3 to 5.9 for roughness and from 1.0 to 1.8 for suction. In general, the TS-wave amplitude will vary during the streamwise evolution of the secondary mode; this amplitude variation is not included in the results of figure 9.

The strong dependence of K_S on ψ_{TS} stems from the need for phase locking between the primary and secondary-modes for parametric resonance. The phase locking was observed in the experiments of Kachanov & Levchenko (1984) and in the numerical simulations of Zang & Krist (1989). Zang & Krist considered the effect of the initial phase of the secondary-mode in plane channel flow. A change in the initial phase (away from the optimum) delays the parametric resonance until the secondary disturbance undergoes a phase adjustment. Downstream the disturbance grows according to secondary-instability theory showing no dependence on the initial phase. The net result of the change in initial phase is an effective change in the initial amplitude. Thus the secondary-mode phase is fixed by the primary mode, and is not arbitrary as for primary instabilities such as TS waves. The excitation of the subharmonic secondary mode stems from the interaction of the acoustic wave with the surface-generated disturbance. This interaction leads to a forcing with a particular phase orientation. For TS-wave receptivity, the forcing phase sets the phase of the excited instability. However, since the secondary-mode phase is set by the primary mode, the forcing phase influences the strength of the receptivity. The strongest forcing occurs when the forced response is in phase with the instability. As the parametric forcing is reduced, $A \to 0$, the dependence on ψ_{TS} is removed.

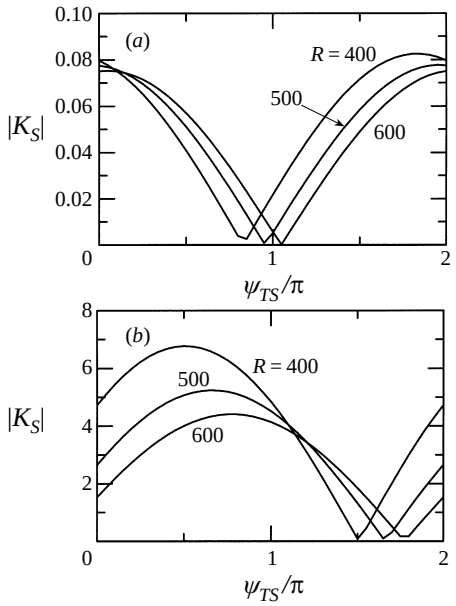

FIGURE 8. Magnitude of the response residue for subharmonic-mode receptivity due to (*a*) roughness, or (*b*) suction, for the conditions $F = 124$, $R = 400$, 500, 600, $b = 0.33$, $A = 0.005$.

5.4. *Relative magnitudes of fundamental and subharmonic modes*

We now consider the potential influence of the receptivity in determining the type of breakdown that occurs in the Blasius boundary layer. The focus is on the scattering mechanisms discussed in §§3 and 4. These are expected to be the dominant mechanisms for relatively quiet free-stream environments. Fundamental modes are excited by a direct scattering of a TS wave due to surface roughness (or suction). For a given TS-wave amplitude and roughness geometry, the fundamental-mode amplitude scales with the roughness height as described by (3.14). The excitation of subharmonic modes involves the scattering of an acoustic wave by the surface roughness (or suction). The subharmonic-mode amplitude, for a given TS-wave amplitude and roughness geometry, scales with the product of the roughness height and the acoustic amplitude, (4.23). Combining (3.14) and (4.23), the fundamental-mode amplitude will be greater than the subharmonic-mode amplitude at the roughness location if

$$|K_F \widetilde{H}(-\mathrm{i}\gamma)| > \epsilon |K_S \widetilde{H}(\hat{\alpha} - \mathrm{i}\gamma)|. \tag{5.3}$$

For comparison purposes, we assume that the Fourier transform evaluated at the two wavenumbers is of similar magnitude. The relative amplitudes of the modes then reduces to a ratio of $|K_F|$ to $|\epsilon K_S|$. Smaller free-stream sound levels provide a bias toward fundamental modes. This is in contrast to the potential role of free-stream vorticity. In wind tunnels with large contraction ratios, the flow may contain high levels of streamwise vorticity. This vorticity may couple directly to the fundamental modes, as suggested by Herbert (1988). Thus an increase in the level of free-stream vorticity may enhance the bias toward fundamental modes.

For the conditions $F = 124$, $R = 606$, $b = 0.33$ and $A = 0.01$, figures 2 and 7 give $|K_F| = 0.0061$ and $|K_S| = 0.058$. The fundamental mode will have the larger initial

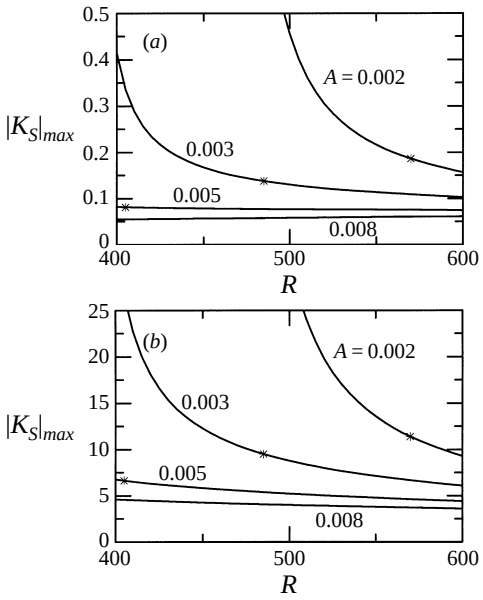

FIGURE 9. Magnitude of the response residue, maximized over the TS-wave phase ψ_{TS}, for subharmonic-mode receptivity due to (*a*) roughness or (*b*) suction for the conditions $F = 124$, $b = 0.33$, $A = 0.002, 0.003, 0.005, 0.008$.

amplitude for acoustic amplitudes ϵ less than 0.1. For the conditions $F = 124$, $R = 606$, $b = 0.33$ and $A = 0.005$, figures 2 and 7 give $|K_F| = 0.0006$ and $|K_S| = 0.074$. For this TS-wave amplitude, the initial amplitude of the fundamental mode will be larger if $\epsilon < 0.008$. These acoustic amplitudes are much greater than those encountered in flight or in wind tunnels. These results show the significant receptivity bias toward fundamental modes. However, the growth characteristics must also be considered in order to understand the relevance of the receptivity bias in effecting transition.

To help generalize the discussion, we consider additional results at the frequency $F = 56$. Figure 10 shows the growth rates for the fundamental and subharmonic modes at $F = 56$, $R = 950$, $b = 0.20$. The fundamental-mode growth rate changes more with the TS-wave amplitude A, but the subharmonic growth rate remains larger over the range of A considered. Figure 11 gives the response residues due to roughness for the fundamental and subharmonic modes. The shape of the curves, and the actual levels, are similar to those for $F = 124$.

We now estimate the relative strength of the fundamental and subharmonic modes at transition for $F = 56$. The localized receptivity occurs after growth of the two-dimensional primary wave. Transition is assumed to occur after a secondary-instability fetch of $\Delta R = 200$. This distance is based on experimental observations: fundamental modes are generally characterized by a shorter fetch than subharmonic modes in the experiments. An approximate n-factor for the secondary modes is given by $N = 2\bar{\gamma}\Delta R$, where $\bar{\gamma}$ is an average growth rate. The fundamental mode will be dominant at transition for acoustic amplitudes

$$\epsilon < (|K_F|/|K_S|)\exp(N_F - N_S), \tag{5.4}$$

where the subscripts on N correspond to fundamental and subharmonic modes. Since the relevant parameters vary weakly with Reynolds number in the neighbour-

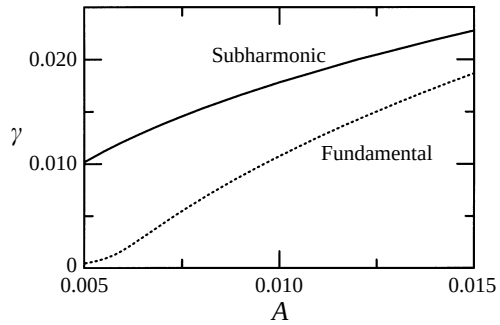

FIGURE 10. Spatial growth rates for dominant fundamental and subharmonic modes at $F = 56$, $R = 950$, $b = 0.20$.

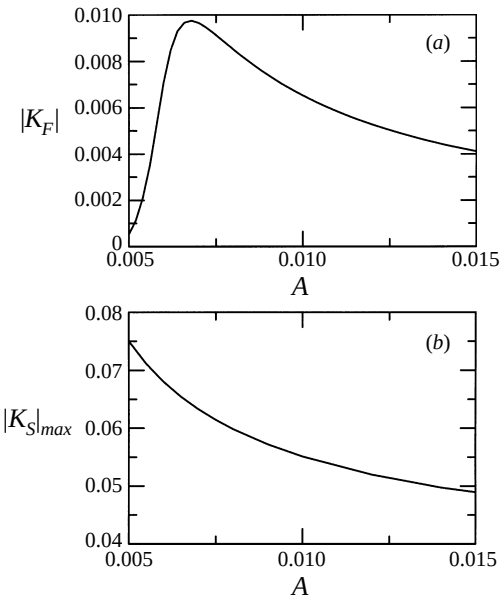

FIGURE 11. Magnitude of the response residue for (*a*) fundamental and (*b*) subharmonic receptivity to roughness at $F = 56$, $R = 950$, $b = 0.20$. Subharmonic response is maximized over the TS-wave phase ψ_{TS}.

hood of the TS-wave branch II, we consider values calculated at $R = 950$. For TS-wave amplitudes of $A = 0.015$ and $A = 0.005$, the fundamental mode will be dominant for $\epsilon < 0.018$ and $\epsilon < 0.00015$, respectively. Yet smaller TS-wave amplitudes will lead to smaller threshold values for ϵ. Therefore, under quiet-tunnel conditions, fundamental modes are expected to be dominant for $A > 0.005$; for $A < 0.005$, subharmonic modes would be dominant. These estimates are based on secondary-mode receptivity due to roughness (or suction) and free-stream acoustic disturbances. Other receptivity sources, such as free-stream vorticity, may play an equal (or greater) role in determining the dominant modes of secondary instability. Nonetheless, the estimates presented here are in general agreement with the observations of Saric & Thomas (1984).

6. Conclusions

The localized receptivity to secondary instabilities has been analysed for both fundamental and subharmonic modes. The fundamental modes are excited through the scattering of the finite-amplitude TS wave. Subharmonic modes are excited through the scattering of an acoustic free-stream disturbance in the presence of the TS wave. The amplitude of the fundamental mode is given by the product of: the roughness height (or suction velocity), the Fourier transform of the surface variation evaluated at the imaginary wavenumber given by the spatial growth rate, and a response residue associated with poles of the secondary instability. The subharmonic mode amplitude is given by the product of: the acoustic amplitude (at the subharmonic frequency), the roughness height (or the suction velocity), the Fourier transform of the surface variation evaluated at the subharmonic-mode wavenumber, and a response residue associated with a pole of the subharmonic instability.

Results show a receptivity bias toward fundamental modes. This bias is overcome for small TS-wave amplitudes due to a reduction in the fundamental-mode receptivity and a reduction in the fundamental growth rate. In flight, or in quiet wind tunnels, fundamental modes are likely to be the dominant mode of secondary instability for TS-wave amplitudes above $A \approx 0.005$ at the receptivity location. For amplitudes below $A \approx 0.005$ subharmonic modes are likely to be dominant.

Calculated receptivity amplitudes for secondary instabilities show a significant dependence on the amplitude of the primary TS wave. For $A < 0.005$, the initial amplitudes of subharmonic modes (maximized over the TS-wave phase) can be 50% smaller than amplitudes estimated from the receptivity of corresponding three-dimensional primary modes. Actual receptivity amplitudes can vary by an order of magnitude depending on the amplitude and phase of the TS wave. For $0.005 < A < 0.008$, the initial amplitudes of fundamental modes can also vary by an order of magnitude depending on A. Over a range of larger TS-wave amplitudes, $0.008 < A < 0.02$, the initial amplitudes of fundamental modes vary by a factor of 2. In practice, a factor of 2 variation in the secondary-mode amplitude may not be important. However, an order of magnitude variation could significantly alter the predicted transition location based on an interaction of primary and secondary modes.

The author has benefited from discussions with Rahul Sen of the Boeing Commercial Airplane Group and from the detailed comments of the reviewers.

REFERENCES

Bertolotti, F. P. & Crouch, J. D. 1992 Simulation of boundary-layer transition: receptivity to spike stage. In *Proc. First Euro. Comp. Fluid Dyn. Conf.* (ed. Ch. Hirsch, J. Périaux & W. Kordulla), pp. 183–190. Elsevier.

Choudhari, M. & Kerschen, E. J. 1990 Instability wave patterns generated by interaction of sound waves with three-dimensional wall suction or roughness. *AIAA Paper* 90-0119.

Choudhari, M. & Streett, C. L. 1992 A finite Reynolds-number approach for the prediction of boundary-layer receptivity in localized regions. *Phys. Fluids* A **4**, 2495–2514.

Choudhari, M. & Streett, C. L. 1994 Theoretical prediction of boundary-layer receptivity. *AIAA Paper* 94-2223.

Craik, A. D. D. 1971 Nonlinear resonant instability in boundary layers. *J. Fluid Mech.* **50**, 393–413.

Crouch, J. D. 1992*a* Non-localized receptivity of boundary layers. *J. Fluid Mech.* **244**, 567–581.

Crouch, J. D. 1992*b* Localized receptivity of boundary layers. *Phys. Fluids* A **4**, 1408–1414.

Crouch, J. D. 1994 Theoretical studies on the receptivity of boundary layers. *AIAA Paper* 94-2224.

Crouch, J. D. & Bertolotti, F. P. 1992 Nonlocalized receptivity of boundary layers to three-dimensional disturbances. *AIAA Paper* 92-0740.

Crouch, J. D. & Herbert, Th. 1993 Nonlinear evolution of secondary instabilities in boundary-layer transition. *Theoret. Comput. Fluid Dyn.* **4**, 151–175.

Crouch, J. D. & Spalart, P. R. 1995 A study of non-parallel and nonlinear effects on the localized receptivity of boundary layers. *J. Fluid Mech.* **290**, 29–37.

Goldstein, M. E. & Hultgren, L. S. 1989 Boundary-layer receptivity to long-wave free-stream disturbances. *Ann. Rev. Fluid Mech.* **21**, 137–166.

Herbert, Th. 1983 Subharmonic three-dimensional disturbances in unstable plane shear flows. *AIAA Paper* 83-1759.

Herbert, Th. 1984 Analysis of the subharmonic route to transition in boundary layers. *AIAA Paper* 84-0009.

Herbert, Th. 1985 Three-dimensional phenomena in the transitional flat-plate boundary layer. *AIAA Paper* 85-0489.

Herbert, Th. 1988 Secondary instabilities of boundary layers *Ann. Rev. Fluid Mech.* **20**, 487–526.

Herbert, Th. & Bertolotti, F. P. 1985 Effect of pressure gradients on the growth of subharmonic disturbances in boundary layers. In *Proc. Conf. Low Reynolds Number Airfoil Aerodyn.* (ed. T. J. Mueller), pp. 65–76. Université Notre Dame.

Herbert, Th., Bertolotti, F. P. & Santos G. R. 1986 Floquet analysis of secondary instability in shear flows. In *Stability of Time-Dependent and Spatially Varying Flows* (ed. D. L. Dwoyer & M. Y. Hussaini), pp. 43–57. Springer.

Herbert, Th. & Crouch, J. D. 1990 Threshold conditions for breakdown of laminar boundary layers. In *Laminar-Turbulent Transition* (ed. D. Arnal & R. Michel), pp. 93–101. Springer.

Kachanov, Yu. S. & Levchenko V. Ya. 1984 The resonant interaction of disturbances at laminar-turbulent transition in a boundary layer. *J. Fluid Mech.* **138**, 209–247.

Kerschen, E. J. 1989 Boundary layer receptivity. *AIAA Paper* 89-1109.

Klebanoff, P. S., Tidstrom, K. D. & Sargent, L. M. 1962 The three-dimensional nature of boundary-layer instability. *J. Fluid Mech.* **12**, 1–34.

Leehey, P. & Shapiro, P. 1980 Leading edge effect in laminar boundary layer excitation by sound. In *Laminar-Turbulent Transition* (ed. R. Eppler & H. Fasel), pp. 321–331. Springer.

Saric, W. S., Reed, H. L. & Kerschen, E. J. 1994 Leading-edge receptivity to sound: experiments, DNS, and theory. *AIAA Paper* 94-2222.

Saric, W. S. & Thomas, A. S. W. 1984 Experiments on the subharmonic route to turbulence in boundary layers. In *Turbulence and Chaotic Phenomena in Fluids* (ed. T. Tatsumi), pp. 117–122. North-Holland.

Singer, B. A., Reed, H. L. & Ferziger, J. H. 1989 The effects of streamwise vortices on transition in the plane channel. *Phys. Fluids* A **1**, 1960–1971.

Tadjfar, M. & Bodonyi, R. J. 1992 Receptivity of a laminar boundary layer to the interaction of a three-dimensional roughness element with time-harmonic free-stream disturbances. *J. Fluid Mech.* **242**, 701–720.

Ustinov, M. V. 1995 Secondary instability modes generated by a Tollmien–Schlichting wave scattering from a bump. *Theoret. Comput. Fluid Dyn.* **7**, 341–354.

Zang, T. A. & Krist, S. E. 1989 Numerical experiments on stability and transition in plane channel flow. *Theoret. Comput. Fluid Dyn.* **1**, 41–64.